Design and Simulation of a High Gain Organic Operational Amplifier for use in Quantification of Cholesterol in Low-Cost Point-of-Care Devices

Munira Raja[1*], David Donaghy[1], Laura Gonzalez-Macia[2], and Antony J. Killard[3]

[1]*Organic Electronics Group, Department of Electrical Engineering and Electronics. University of Liverpool. Brownlow Hill. Liverpool L69 3GJ. United Kingdom*

[2]*Ecole Nationale Supérieure de Chimie de Paris (Chimie ParisTech), 11 Rue Pierre et Marie Curie, 75005, Paris, France*

[3]*Biomedical Science Group, Department of Applied Sciences. University of the West of England. Frenchay Campus, Coldharbour Lane, Bristol BS16 1QY. United Kingdom*

[*]*Email: mraja@liv.ac.uk*

Abstract: This paper presents circuit design and simulations of a high gain organic Op-Amp, for use in quantification of real cholesterol, in the range of 1-9 mM. A 7-stage inverter chain is added onto the design so as to enhance the amplifier gain. The circuit adapts PMOS design architecture with saturated loads, simulated on a conventional platform, using appropriate OTFT model and associated parameters. The effect of variation in threshold voltage on circuit operation is also examined. For a supply voltage of ±15 V, the DC output voltage is found to be within an acceptable range of -1 V to -12.5 V, with a highest open loop gain of 83 dB. The closed loop gain is also in agreement with theoretical values, in the range of 1.5 dB to 39 dB, with corresponding bandwidths of 770 Hz to 275 Hz respectively. The latter gain of 39 dB and/or gain-bandwidth product of 10.63 kHz is currently the highest reported in the literature, for this lower supply voltage. The amplifier offers adequate quantification factor, with linear sensitivity of -0.7 V/mM. This paper is the first to adapt organic circuit designs in quantification of cholesterol, with promising outputs, for implementation in low-cost sensor systems.

1 Introduction

Organic Electronics continues to emerge as a technology for flexible, high-volume and low-cost systems. Over the past decade, the development of organic circuits, particularly for digital systems [1-5], has continued to evolve steadily, however a more gradual improvement has been observed for the analog counterpart [6-11]. The development of the latter has been more challenging, due to the complexity of the fabrication processes [9], low charge carrier mobility and instability of the organic semiconductors [12-19]. Nonetheless, efforts have continued to develop simpler analog circuits, with minimal number of organic thin-film transistors (OTFTs), including digital-to-analog converters (DAC) and operational amplifiers (Op-Amp). Such analog circuits are gaining huge interest for implementation in smart sensor systems, for example in point-of-care diagnostics, where there is a growing need for regular monitoring of personal health, so as to identify any health issues at an early stage. The opportunities have also been aided by the flexible nature of the technology on offer [20-24], compatibility with biological materials, and possibility of high volume manufacturing at low-costs. In order to implement organic Op-Amp in sensor systems, the optimum operational conditions required include high gain and/or gain-bandwidth product, so as to generate a sufficient output voltage range. The bandwidth of the Op-Amp, is not considered to be a critical requirement, however adequate values in the range of few hundreds of Hz may be desirable. Moreover, the supply voltage needs to be within a practical range so as to utilise smaller area on the substrate. Equally important, is the design architecture used for the circuit, as this defines the processing steps, which needs to be minimised so as to enhance the overall circuit yield and reduce costs. Table 1 summarises the organic amplifier designs reported so far in the literature [6, 8, 24-28], with respective key performance features and design architectures. The highest closed loop gain presented is 42 dB [25], however with a low operational bandwidth of 75 Hz. This subsequently results in a low gain-bandwidth product of only 3.75 kHz and thus a lower output voltage range. To compensate for this, a larger supply voltage is utilised, which also accommodates for the low charge carrier mobility of the organic semiconductor. In terms of the design architecture, CMOS is traditionally

known to have attractive attributes however implementing such architecture in organics [6, 25, 29] is challenging due to its complex processing steps. For example, for CMOS architecture, an additional input gate is required for every inverter in order to control the different threshold voltages. Moreover, different metals are required for the source and drain contacts, of the p-type and n-type OTFTs. Alternatively, the pseudo-PMOS (p-channel transistors only) architecture [9, 26, 27, 28] has been commonly adapted, due to simpler processing steps and higher mobility of the available p-type semiconductors.

	Closed loop gain, A_{CL} (dB)	Open loop gain, A_{OL} (dB)	Unity gain bandwidth (Hz)	Bandwidth (Hz)	Gain-Bandwidth product (kHz)	Supply Voltage (V)	Organic circuit technology
Our paper	39	83	770	275	10.63	30	PMOS
[6]	27	Unknown	Unknown	70	1.9	80	CMOS
[9]	15	23	10k	10k	13	15	PMOS
[25]	42	50	Unknown	75	3.75	50	CMOS
[26]	30	20	10k	10k	30	15	PMOS
[27]	27	27	600	Unknown	13.2	40	PMOS
[27]	22	22	1.02k	Unknown	13.4	40	NMOS
[28]	Unknown	36	7.5	7.5	0.47	5	PMOS
[29]	Unknown	23	Unknown	Unknown	Unknown	Unknown	CMOS

Table 1: Summary of the state-of-the-art in the development of organic amplifiers.

In this work, we propose appropriate approaches in the design and simulation of the organic analog circuit, for use in quantification of real cholesterol in the range 1 – 9 mM. The circuit comprises of an organic Op-Amp, in connection with an inverter chain, so as to boost the gain and/or gain-bandwidth product, and a latch to amplify and enable the output current. The circuit operates with a relatively low supply voltage of ±15 V, and generates adequate output voltage range, for the proposed application; namely quantisation of cholesterol levels. The design utilises saturated PMOS architecture, simulated on a Cadence platform, with the aid of appropriate experimental organic OTFT parameters and model, derived and validated

elsewhere [30-32]. From the simulation, key outputs including voltage range, bandwidth and overall gain are determined, with respect to fluctuation in the threshold voltage, which is a common concern in the field. Subsequently, the functionality of the circuit, in connection to cholesterol sensing is demonstrated. The circuit designs offer practical outputs including high gain-bandwidth product, lower supply voltage and appropriate design architecture, to allow its implementation as a key functional block in low-cost smart sensor systems. This paper is organised as follows: Section II provides the methodology, commencing with an overview of the integrated cholesterol sensor system, and subsequently input and output specification of the organic circuit design, and defining the OTFT model and parameters. Section III presents the simulation results of the Op-Amp, and discusses the effect of adding an inverter chain and a latch. Subsequently, the functionality of the overall circuit in quantification of cholesterol is presented, and finally, section IV draws the conclusion.

2 Methodology

2.1 System overview and organic circuit input/output specifications

To establish the design architecture for the organic circuit, it is essential to initially describe the functionality of the integrated sensor system, for use in semi-quantitative measurement of the cholesterol levels. The system, labelled here as SIMS i.e. Smart Integrated Miniaturised Sensor System, and depicted in Fig. 1a, comprises of mainly printed components such as an electrochemical cell, battery, and electrochromic display, and an organic circuit, as shown by respective real images. The three printed components were successfully integrated on a same substrate, using compatible processes, whilst the organic circuit was to be designed and developed on a separate substrate. Ulitmately, all of the components were to be integrated on a same flexible substrate, using minimal number of steps, so as to maintain low processing costs.

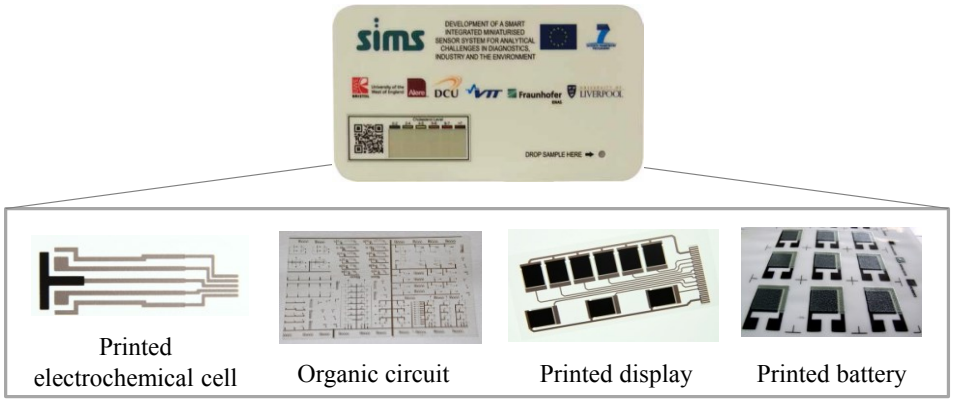

(a)

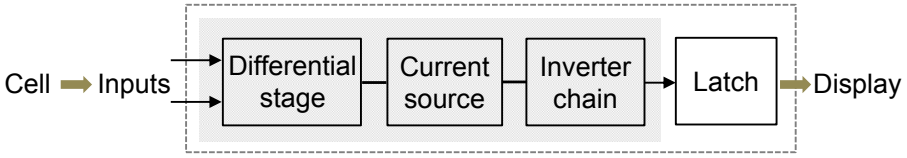

(b)

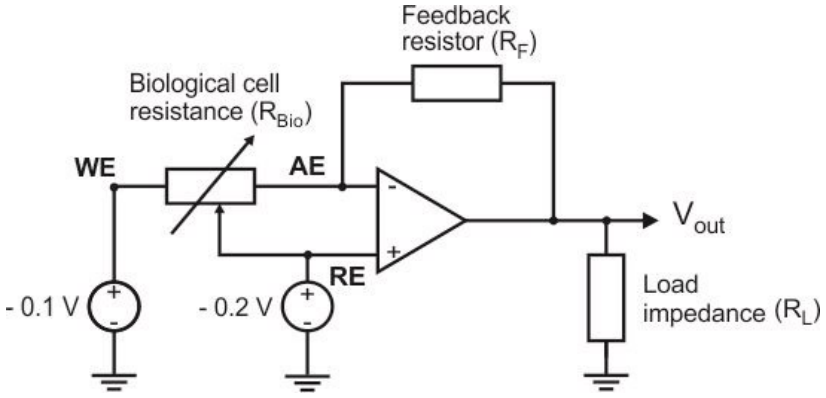

(c)

Fig. 1 *Integrated smart sensor system with respective organic circuit.*

(a) Sensor system for semi-quantitative measurement of cholesterol comprising of real printed electrochemical cell, organic circuit, printed display, and printed battery.

(b) Block diagram of the organic circuit including an Op-Amp (shaded) comprising of differential amplifier, current source and inverter chain, connected to a latch.

(c) Schematic diagram of an inverting Op-Amp with respective input connected to the electrochemical cell terminals. R_{Bio} represents input resistance between 276 kΩ to 1.38 MΩ, corresponding to cholesterol of 9 - 0 mM respectively.

The input of the organic circuit is connected to the electrochemical cell, whilst the output to the electrochromic display bars (i.e. non-numeric). When blood sample containing cholesterol is introduced onto the electrochemical cell, the organic circuit computes the level of cholesterol present in terms of charge, and subsequently generates an ouput voltage. The magnitude of this voltage depends on the level of cholestrol present in the sample. This voltage is then fed onto a latch, which is connected to the display bars. Depending on the voltage attained from the circuit, respective bars turn on. The range of cholesterol corresponding to the bars (× 6) are 0 – 2 mM, 2 – 4 mM, 4 – 5 mM, 5 – 6 mM, 6 – 7 mM and > 7 mM respectively. Figure 1b shows the block diagram of the organic circuit to be designed and simulated. Detailed discussions on the designs of the other sensor components are beyond the scope of this paper.

The circuit comprises of an organic operational amplifier (Op-Amp) consisting of differential stage and current source, with added inverter chain, connected to a latch. The schematic diagram of the Op-Amp is as depicted in Fig. 1c, with its input connected to the output of the printed electrochemical cell, comprising of three terminals, namely Reference (RE), Working (WE) and Auxiliary (AE) electrodes. For accurate operation of the cell, the voltages at the reference and working terminals need to be fixed at - 0.2 V and - 0.1 V respectively [33]. Typically, this results in a potential difference of 0.1 V between the terminals, assuming no current is drawn by the reference electrode. Due to such voltage requirements of the cell, the operating point of the Op-Amp needs to be shifted, from a theoretical zero to - 0.2 V. Furthermore, in order to define the input impedance of the Op-Amp, the resistance of the cell is determined by measuring the variation of the current with changes in cholesterol levels. The cholesterol sample comprises of phosphate buffered saline (PBS)/triton solution added onto 100 U/mL enzyme cholesterol oxidase (ChOx). This method measures free cholesterol rather the ratio of high to low density lipoprotein cholesterol [34]. The measurements are taken after a settling time of 400 seconds, to allow the current from the cell to stabilise to a steady-state, followed by a reaction time of 180 seconds. Subsequently, such timing defines the bandwidth of the sensor, which is not considered here to be a key design parameter, and

thus a bandwidth of > 1Hz is deemed to be sufficient. From the measurements in Fig. 2, the current is found to range between 220 – 500 nA for cholesterol levels of 0 – 9 mM, which corresponds to resistance, referred hereafter as R_{Bio}, in the range of 276 kΩ – 1.38 MΩ, with the highest resistance corresponding to no cholesterol in the cell.

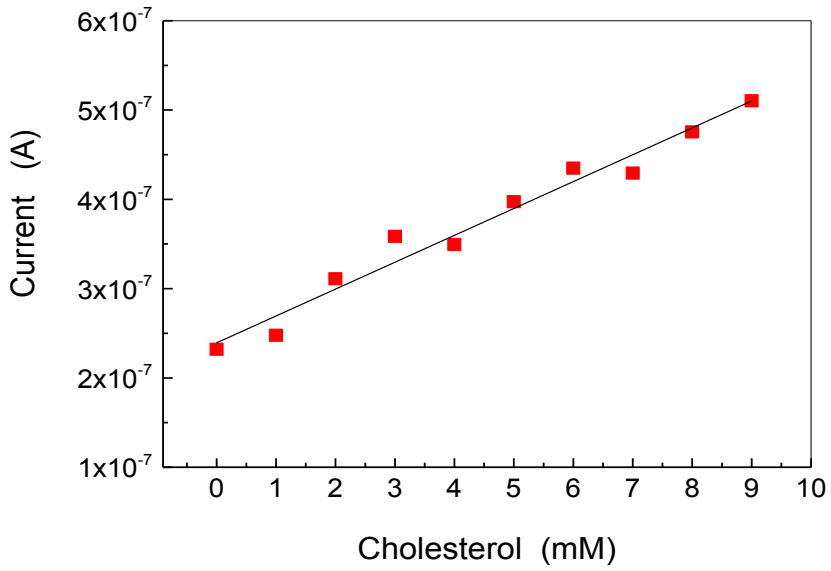

Fig. 2 *Current measured from electrochemical cell with changes in concentration of free cholesterol. The current corresponds to resistance R_{Bio} between 276 kΩ to 1.38 MΩ (no cholesterol).*

For sensing applications, the closed loop gain A_{CL} and/or the gain-bandwidth product of the Op-Amp are considered to be key parameters. The variable resistor R_{Bio} in Fig. 1c, represents the input impedance, which defines the amount of cholesterol present in the sample. When cholestrol is added onto the cell, the organic Op-Amp siginifies a change in R_{Bio} and subsequently generates a corresponding output voltage V_{out}. The load resistor R_L relates to the impedance of the display, and the external feedback resistor R_F establishes the theoretical minimum and maximum output voltages. It can be shown that the closed loop gain of the circuit is given by Eq. 1, where V_{WE} and V_{AE} are voltages at the working and auxiliary terminals respectively.

$$A_{CL} = \frac{V_{out}}{V_{in}} = \frac{V_{AE}}{V_{in}}\left(1 + \frac{R_F}{R_{Bio}}\right) - \frac{R_F}{R_{Bio}} = 2 + \frac{R_F}{R_{Bio}} \quad (1)$$

For accurate operation of the cell, the voltages need to be fixed at V_{in} = V_{WE} = - 0.1 V and V_{AE} = - 0.2 V, with R_{Bio} varying between 276 kΩ to 1.38 MΩ. With a supply voltage of ± 15 V, the maximum theoretical output voltage is -15 V, which would subsequently yield a maximum A_{CL} of 146 (or 43 dB). However, assuming a value of R_F to be 22 MΩ, this results in A_{CL} in the range of 81.7 – 17.9, with respect to the range of R_{Bio} given above. These values will be compared later with the simulation results on the Op-Amp, taking into consideration appropriate parameter values of the OTFTs on the PMOS designs, including low charge carrier mobility and variation of the threshold voltage. In regard to the output impedance, the output of the organic circuit is connected to the electrochromic display comprising of 6 bars. For accurate operation of the electrochromic display, a nominal voltage of 1.1 V and current of 25 μA are required to turn-on the bars and maintain sufficient luminescence respectively. With such input and output specifications, respective designs for the organic circuits are discussed and simulation results presented in the next sections.

2.2 OTFT Model and Parameters

Prior to discussions on the simulation results of the respective circuit block designs, it is essential to consider the tools that are to be utilised in the accurate simulation of such designs. Typically, organic circuits are simulated by editing existing silicon model and parameters on a conventional platform, so as to accommodate the properties of the OTFT. In this paper, we follow this approach and utilise Cadence circuit simulator (V.5.10). The revised model, referred hereafter as the OTFT model, is illustrated in Fig. 3a and expressed by Eq. 2 and Eq. 3, operating under unsaturated and saturated regimes respectively. The models comprise of the drain current attributed with the silicon model, with added current components, through a Verilog file, to take into account the properties of the organic

transistor, including the higher power dependency of the gate and drain voltages, as commonly observed in OTFT models [30], [31].

$$I_{DS\_unsat} = I_{DS\_silicon\_unsat} + K_{drift}[(V_{GS} - V_{TH})^{c_{drift}+1} - (V_{GS} - V_{TH} - V_{DS})^{c_{drift}+1}] \quad (2)$$

where,

$$I_{DS\_silicon\_unsat}(V_{GS}, V_{DS}, R_S, R_D) = \beta\left\{(V_{GS} - I_{DS}R_S - V_{TH})\left(V_{DS} - I_{DS}(R_S + R_D)\right) - \frac{\left(V_{DS} - I_D(R_S + R_D)\right)^2}{2}\right\}$$

And,

$$I_{DS\_sat} = I_{DS\_silicon\_sat} + K_{drift}[(V_{GS} - V_{TH})^{c_{drift}+1} - (V_{GS} - V_{TH} - V_{DS})^{c_{drift}+1}] \quad (3)$$

where,

$$I_{DS\_silicon\_sat}(V_{GS}, R_S) = \beta(V_{GS} - I_{DS}R_S - V_{TH})^2$$

Here I_{DS} is the drain current of the OTFT under saturated and unsaturated regime, β is the device constant, $I_{DS\_silicon}$ is the drain current associated with the silicon model, V_{DS} and V_{GS} are the drain-source and gate-source voltages, R_S and R_D are the contact resistances associated with the source and drain contacts, V_{TH} is the drift threshold voltage, and, K_{drift} and c_{drift} incorporates the material and device constants of the OTFT operating under drift condition. As it can be observed, the model takes into account the contact resistance effect, in the form of sheet resistance, such that $R_{sh}/W = R_D = R_S$, where W is the channel width of the transistor. However, it should be noted that the contact resistance effect was taken into account within the silicon model only, and not within the added Verilog current component.

Using the expressions above, key parameter such as the threshold voltage can be extracted from experimental data of solution-based 6,13-bis(tri-isopropylsilylethynyl) pentacene (TIPS) OTFT, of structure as in Fig. 3b. Here, aluminium (Al) is used as the gate contact and aluminium oxide (Al_2O_3) as the gate dielectric with a relative permittivity of 10 and thickness of approximately 45 nm. Gold (Au) is used for the source and drain contacts, which consequently has high source/drain (contact) resistance in the range of 240 kΩ to 24 MΩ, corresponding to channel widths of 10 mm to 100 μm respectively. The transfer

characteristics above and below threshold, are as shown in Fig. 4a and Fig. 4b, for a channel length *L* of 100 μm and channel width *W* of 2 mm, with drain voltages of -1 V and -10 V respectively. These drain voltages were chosen so as to allow extraction of the value of the threshold voltage, under diffusion and drift regimes, which were found to be approximately -0.75 V and -1.5 V respectively. Such threshold voltages are commonly observed in polycrystalline OTFTs [30], [35], and are essential in OTFT modelling, particularly at low voltages where the leakage current dominates.

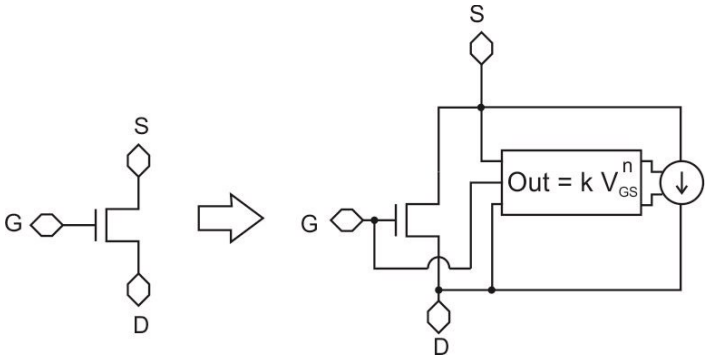

(a)

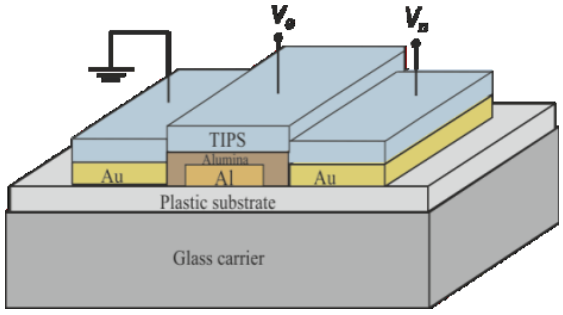

(b)

Fig. 3 *Model and structure of the OTFT*

(a) Conventional model (left) with added features to account for organic characteristics, resulting in appropriate OTFT model (right) for simulation.

(b) Cross-section structure of the TIPS OTFT, with Al_2O_3 as the gate dielectric and Au as source/drain contacts.

Using the extracted value of the threshold voltage under drift regime V_{TH}, other key parameters such as K_{drift} and c_{drift} were determined at approximately 7×10^{-12} (SI units) and c_{drift} of 2.8 respectively, and subsequently utilised in model [30], so as to generate better fits between the model and data. As it can be noted, the value for c_{drift} is slightly higher compared to that of silicon, corresponding to the power exponent on the voltages of typically 2.

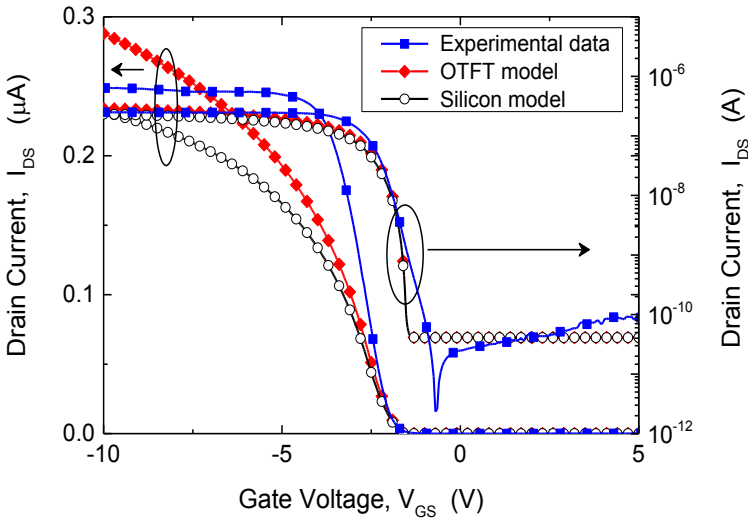

(a)

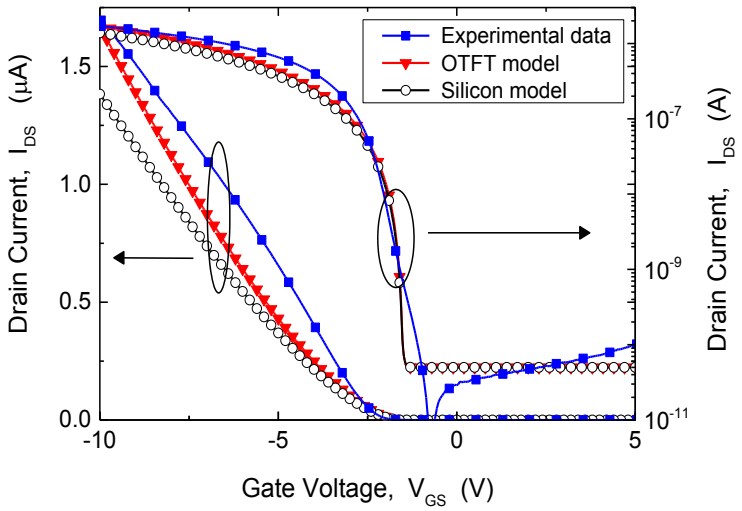

(b)

Fig. 4 *Fits of the sub-threshold plots and transfer characteristics of TIPS OTFT, to the standard silicon and revised OTFT model at drain voltage of (a) - 1 V and (b) - 10 V.*

The plots in Fig. 4 also show fits of the data using both silicon and TIPS OTFT models, assuming a field-effect mobility for both, of 0.035 $cm^2V^{-1}s^{-1}$. This value is lower than those reported in the literature; however it is more practical since the reported values are extracted from individual transistors rather than circuits, where the mobility is expected to decline, due to the additional processing steps. As expected the OTFT model shows better agreement with the experimental data than the silicon model, at both low and high drain voltages. Some deviation in the fits is also observed, particularly at low drain voltages, which is believed to be associated with the high contact resistance on the source. At low drain voltage, the contact resistance is pronounced, and a higher error is observed between the model and data, however as the drain voltage increases with respect to the source, the error reduces due to a decrease in the resistance. As indicated earlier, the model does take into account the contact resistance effects through the silicon model in terms of sheet resistance. The divergence observed could be associated with the lack of contact resistance component, within the added model (in Verilog), which could have potentially under estimated the resistance values and thus drive current of the OTFT. Nonetheless, the divergence are deemed plausible, and justifies the application of the proposed model, in generating accurate simulation of the organic circuit designs, as discussed in the next section.

3 Circuit design and simulation

3.1 Differential Amplifier

Referring to Fig. 1(b), the simulation commences with the differential amplifier with saturated loads, comprising of a differential stage and a current source, with OTFTs labelled M1 to M5 and M6 to M8 respectively, as in the schematic diagram in Fig. 5a, for a supply voltage of ±15 V. It can be shown that the single output voltage of the differential amplifier can be represented by Eq. 4 [36], where β_{M1} and β_{M4} are the drive constant of devices M1 and M4 respectively, V_{indf} is the input voltage difference between negative input *in-* (AE) and positive

input *in*+ (RE) terminals, I_{DM5} is the bias current through M5, and V_{SS} is connected to the negative terminal of the supply rail at - 15V.

$$V_{out} = \left(\frac{\beta_{M1}}{4\beta_{M4}}\right)^{0.5}\left(V_{indf} - 2\left(\frac{\beta_{M4}}{\beta_{M1}}\right)^{0.5}(V_{TH} - V_{SS}) + \sqrt{\frac{4I_{DM5}}{\beta_{M1}} - \left(V_{indf}\right)^2}\right) \quad (4)$$

And the gain of the differential amplifier is defined by Eq. 5, which suggests that a maximum gain is attained when V_{indf} approaches zero.

$$\text{Gain}_{DA\_DC} = \left(\frac{\beta_{M1}}{\beta_{M4}}\right)^{0.5}\left(1 - \frac{V_{indf}}{\sqrt{\frac{4I_{DM5}}{\beta_{M1}} - {V_{indf}}^2}}\right) \quad (5)$$

The bias current I_{DM5} is set at 1.8 µA, which corresponds to a gate to source voltage V_{GS} of -3.5 V. By reducing the bias current, the drain to source voltage V_{DS} across M5 is also reduced, which subsequently increases the final output voltage swing. The magnitude of this voltage from the differential amplifier is dictated by the V_{DS} of M5 as well as the difference in the aspect ratios between M1/M2 and M3/M4 respectively. The aspect ratios of M3 (M4) dictate the final output voltage of the differential amplifier, and are required to be large enough so as to sink the current supplied by M5. Moreover, the aspect ratio of M1 dictates the speed at which M1 (M2) can react to the changes in the input voltage i.e. slew rate. In such case, the differential amplifier can be observed to have a maximum gain of $(\beta_{M1}/\beta_{M4})^{0.5}$. Such that for a gain of 10, the width of M1 needs to be 100 × greater than that of M4. Assuming *W*/*L* of M1 = M2, M3 = M4, M5 = M6 and M7 = M8 of respective dimensions as represented in Fig. 5a, the DC output voltage of the differential amplifier is simulated, with the aid of the OTFT model discussed earlier, for drift threshold voltages V_{TH} of -1.5 V and -2.5 V. Figure 5b shows the variation of the output against input voltages of the differential amplifier, with respective minimum and maximum output voltages at -2.5 V and -13.4 V for

V_{TH} = -1.5 V, and -2.6 V and -12.4 V for V_{TH} = -2.5 V respectively. As the threshold voltage increases, the maximum output voltage reduces, and the switching point shifts slightly by 350 mV, which is thought to be associated with the reduction in the drive current of the OTFTs. Moreover, the output voltage range for both cases corresponds to approximately 73% of the maximum theoretical value of -15 V, and a differential gain of 1 and 1.4 respectively as from Fig. 5c. Such reduced values of the voltage swing and gain are believed to be attributed to the design architecture comprising of saturated loads, low charge carrier mobility and high contact resistance. Nonetheless, if the input voltage is taken within the range of ±3 V, then the gain is approximately 1.5 for both threshold voltages. Such gain values are within reasonable agreement with the theoretical value of 1.6 (or 4 dB), as estimated from Eq. 5.

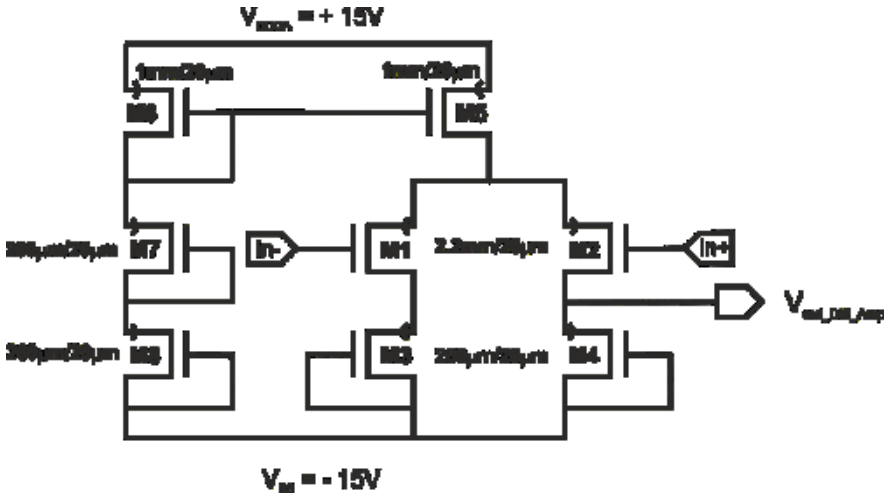

(a)

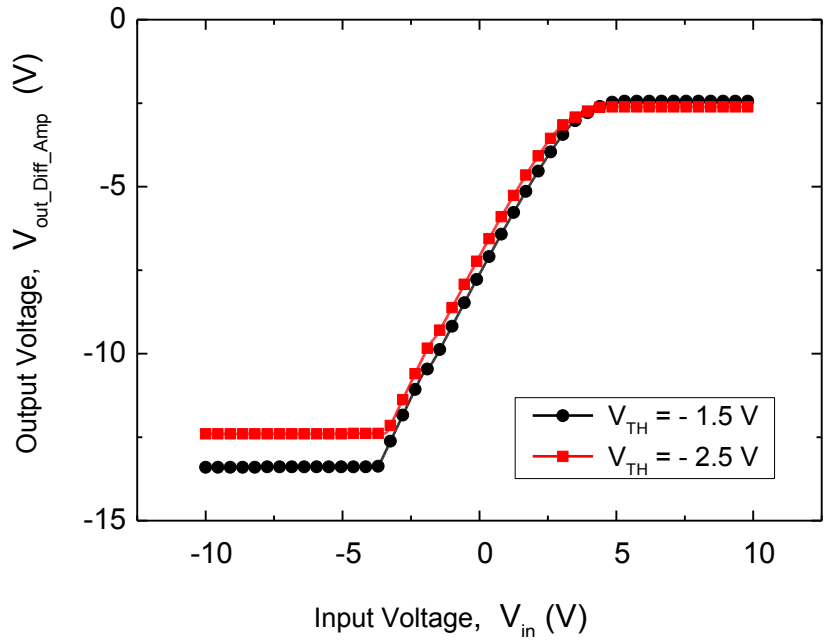

(b)

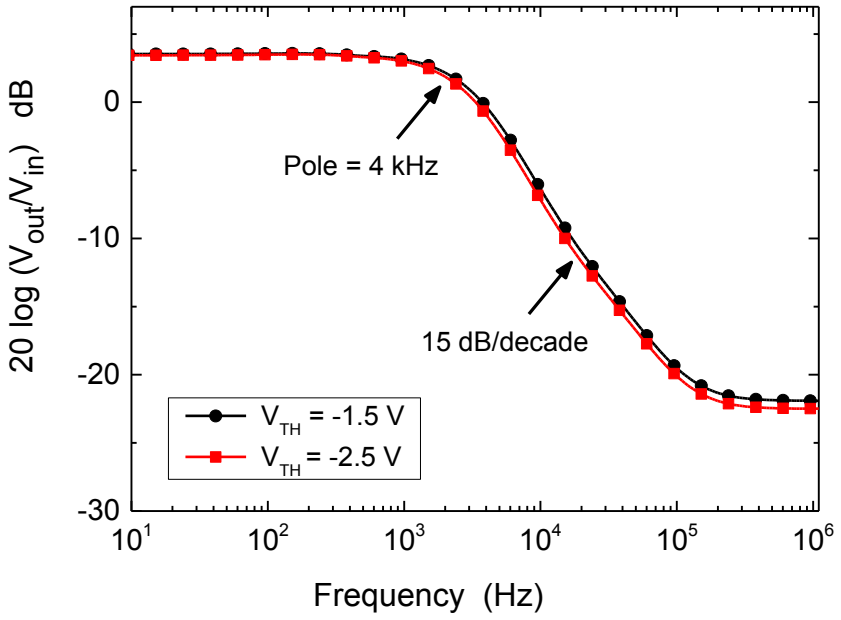

(c)

Fig. 5 *Organic Differential Amplifier*

(a) Schematic diagram comprising of a differential stage with OTFTs M1 to M5, and current source with OTFTs M6 to M8.

(b) Simulation of the output against input voltages, for different threshold voltages, with voltage on the positive terminal set to -0.2 V.

(c) Simulation of the frequency response with changes in threshold voltage, resulting in open loop gain of 4 dB, bandwidth of 4 kHz, and thus gain-bandwidth product of 16 kHz.

The frequency response of the gain of the differential amplifier is given by Eq. 6 [37], where C_{gdM2}, g_{mM2}, g_{dsM2} are the gate to drain capacitances, transconductance and output conductance for transistor M2 respectively, C_{gsMd1} and C_{gsM4} are the gate to source capacitance of M_{d1} and M4 respectively, and g_{mM4}, and g_{dsM4} refer to the transconductance and output conductance of transistor M4 respectively. The value of R_{M2M4} is the inverse sum of g_{dsM2}, g_{dsM4} and $g_{mM4.}$ The bandwith of the amplifier is dictated by the poles and zeros, which are determined by g_{mM2}/C_{gdM2} and $-1/R_{M2M4}$ (C_{gdM2}+C_{gsM1}+C_{gsM3}) respectively.

$$Gain_{DA\_AC} = \frac{-g_{mM2}R_{M2M4}\left(1-s\frac{C_{gdM2}}{g_{mM2}}\right)}{1+sR_{M2M4}\left(C_{gdM2}+C_{gsM4}+C_{gsM19}\right)} \quad (6)$$

Figure 5c indicates a 15 dB/decade roll-off for both values of threshold voltages, since the pole is unchanged in the M1:M3 branch of the circuit. The pole frequency of the circuit agrees with the theoretical value of 3.6 kHz with a 15 dB/decade roll off. The unity bandwidth is approximately 4 kHz for V_{TH} of -1.5 V, which reduces slightly as the threshold voltage is increased, due to the associated reduction in the transconductance g_m. The open loop gain is found to be 4 dB, with a corresponding gain-bandwidth product of 16 kHz. In order to boost the gain of the amplifier, an inverter chain is added as discussed in the next section.

3.2 Addition of an Inverter Chain

To increase the overall gain of the organic Op-Amp, and counteract the change in the switching voltage of the differential amplifier, an inverter chain is added after the differential amplifier stage. The gain of a saturated load inverter is given by Eq. 7 [37], where the term *i* relates to an inverter stage and *j* to the next inverter in the chain.

$$Gain_{inv\_AC} = \frac{-g_{m\_driver\_i} \times R_{invout\_i}\left(1 - s\frac{C_{gd\_driver\_i}}{g_{m\_driver\_i}}\right)}{1 + sR_{invout\_i}\left(C_{gd\_driver\_i} + C_{gs\_load\_i} + C_{gs\_driver\_j}\right)} \quad (7)$$

Here g_{m_driver} is the transconductance of the driver, C_{gd} is the gate-drain capacitance, C_{gs} is the gate-source capacitance, and $R_{invout} = 1/g_{m\_load}$. Simulation of the Op-Amp with a 7-stage inverter chain of schematic diagram as in Fig. 6a was carried out. Respective aspect ratios for the OTFTs are as shown in the diagram, and were chosen so as to shift the switching point of the amplifier to -0.2 V by increasing the gain, which was required for accurate operation of the electrochemical cell.

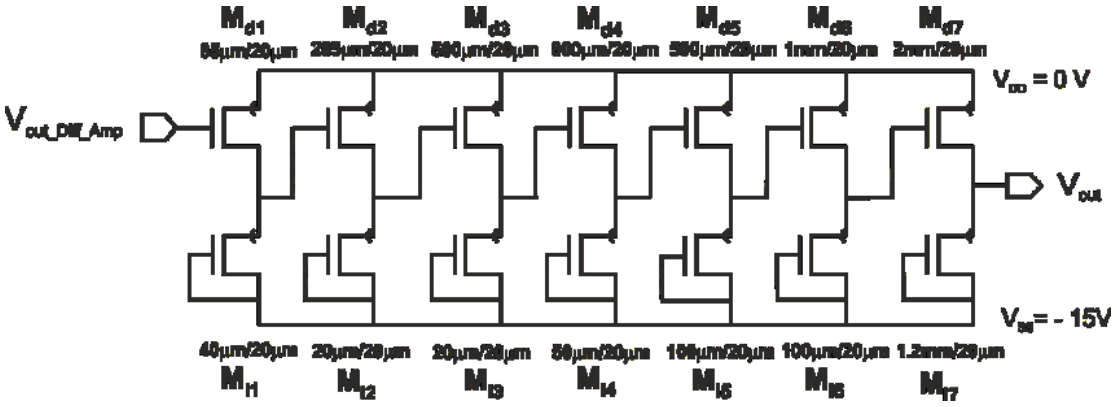

(a)

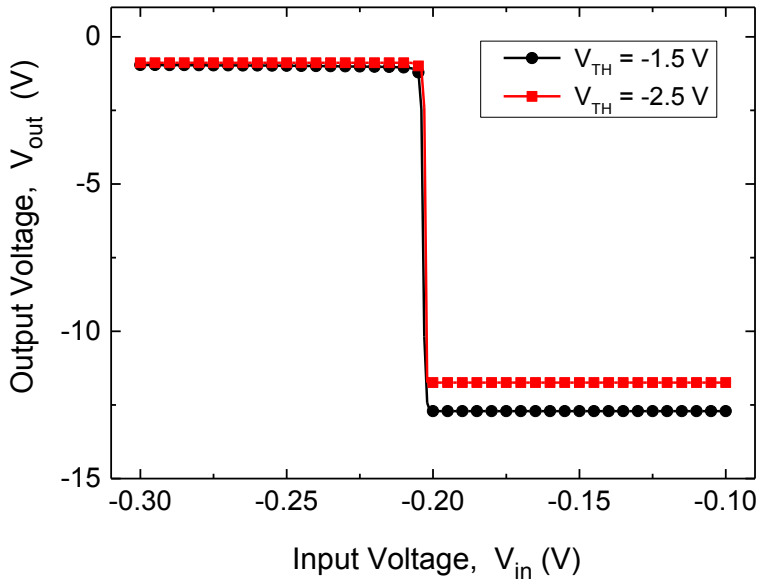

(b)

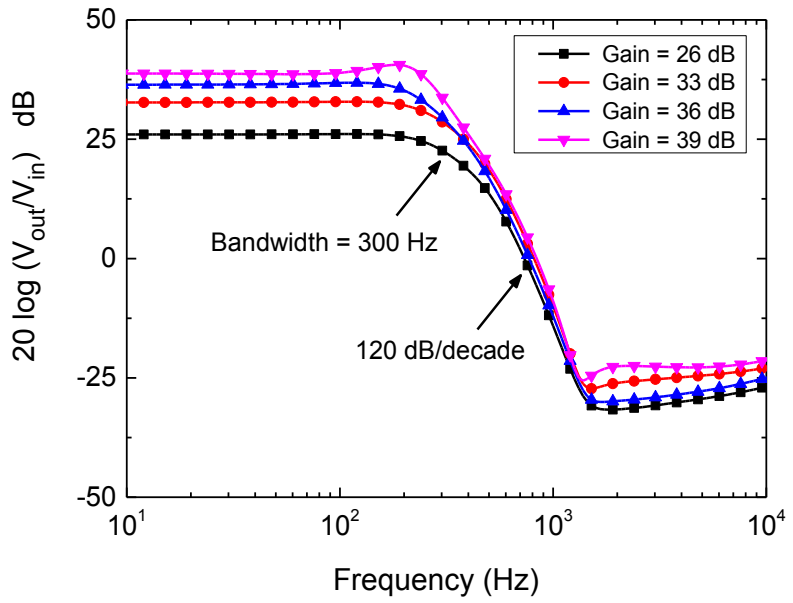

(c)

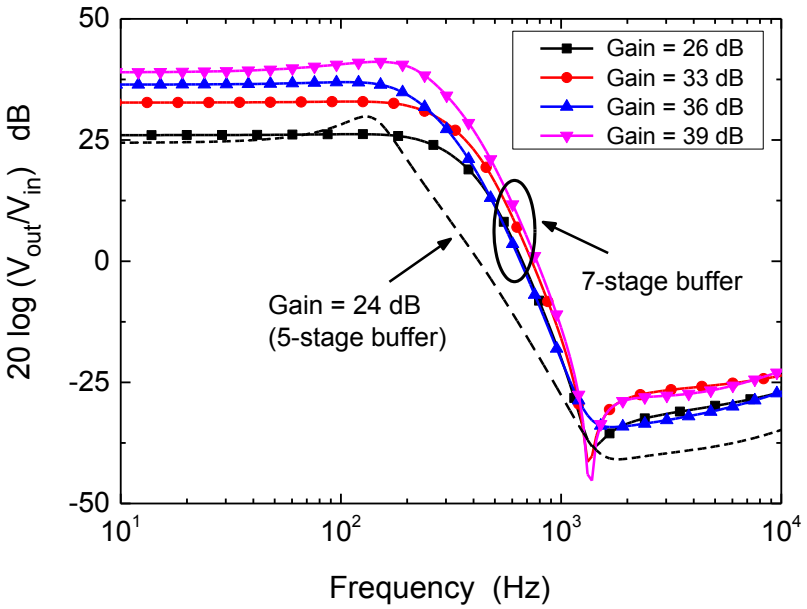

(d)

Fig. 6 *Organic Differential Amplifier with 7 stage inverter chain*

(a) Schematic diagram of a 7-stage inverter chain with saturated loads, connected to the output of the differential amplifier.

(b) Simulation of the output voltage of the organic Op-Amp with inverter chain, with respect to changes in threshold voltage. The switching point is at - 0.2 V and output voltage reduces with higher threshold voltage.

(c) Simulation of the frequency response of the organic Op-Amp with inverter at V_{TH} = -1.5V.

(d) Simulation of the frequency response of the organic Op-Amp with inverter at V_{TH} = -2.5V.

Figure 6b shows the corresponding variation of output voltage with respect to the input voltage, with threshold voltages of -1.5 V and -2.5 V respectively. For both voltages, the switching point is found to be nearly the same, at a fixed input value of -0.2 V. For a threshold voltage of -1.5 V, the output voltage range is found to be from -1 V to -12.5 V, which is 77 % of the ideal range. As observed earlier in the differential stage, this output voltage range is slightly higher (by 0.95 V), compared to when the threshold voltage is -2.5 V. For comparisons, simulations were also carried out on a 5-stage, 7-stage and 9-stage inverters, which resulted in respective open loop gain A_{OL} of the Op-Amp of 913 (59 dB), 14k (83 dB) and 100k (100 dB) respectively. It should be noted that with increasing number of OTFTs in larger inverter stages would impact the circuit yield. Thus, the 7-stage inverter was selected for integration onto the Op-Amp design due to its adequate gain for sensor application, and potentially better yield compared to a 9-stage inverter chain. Figures 6c and 6d show the frequency response of the Op-Amp with inverter stages, for different threshold voltages respectively. As expected, the gain increases as the bandwidth reduces for an overall system range, with R_{Bio} between 276 kΩ to 1.38 MΩ, corresponding to cholesterol of 0 - 9 mM. Here, the feedback resistance R_F = 22 MΩ and load resistance R_L = 1 GΩ, with the latter reflecting the input gate capacitance of an OTFT. The inverter stages add additional gain, and also provide ample stability within the closed loop response. The maximum operational frequency, is found to be 302 Hz for V_{TH} = -1.5 V, and 280 Hz for V_{TH} = -2.5 V, attained at a gain of 26 dB. The highest open loop and closed gains are 83 dB and 39 dB respectively, at a frequency of 275 Hz, for both threshold voltages, with a gain-bandwidth product of approximately 10.6 kHz. Table 2 gives the summary of the closed loop gains and loop gains with corresponding bandwidths, with respect to changes in cell resistances. The bandwidth also depends on the number of inverter stages, as observed in Fig. 6d, such that as the number of stages reduces from 7 to 5, the bandwidth also reduces from 280 Hz to 190 Hz, for a gain of 26 dB. Moreover, the closed loop gain of the amplifier with a 5-stage inverter is found to be 2 dB lower than the theoretical value of 26 dB i.e. at 24

dB. Each inverter stage in the final design inserts a pole which degrades the frequency response of the final amplifier to 120 dB/decade, with each pole frequency determined by Eq. 7.

Cell resistance R_{Bio} (kΩ)	Loop gain (dB)	Closed loop gain (dB)	V_{TH} = - 1.5 V		V_{TH} = - 2.5 V	
			Bandwidth (Hz)	Gain-Bandwidth product (kHz)	Bandwidth (Hz)	Gain-Bandwidth product (kHz)
1225	57	26	302	7.85	280	7.28
516	50	33	288	9.43	275	9
360	47	36	239	8.73	218	7.97
253	45	39	275	10.63	275	10.63

Table 2: Amplifier outputs extracted from Fig. 6c and Fig. 6d for a differential amplifier with a 7-stage inverter chain for R_F = 22 MΩ and R_L = 1 GHz.

3.3 Use of a Latch

With regard to the output specification discussed earlier, the output resistance of the Op-Amp is considered to be insignificant due to the feedback topology, and thus the loading effect of the display on the output is insignificant in this application. As highlighted earlier, a current of ≥ 25 μA is required to drive the display bars. To achieve this, an output latch is utilised, of schematic diagram as in Fig. 7a, which comprises of inverter stages with saturated load, and an enabled clock (M7), with respective aspect ratios as highlighted in the diagram. Such values of the aspect ratio were chosen so as to eliminate the threshold voltage dependency and to supply a maximum current of 25 μA as required for accurate operation of the display elements. Moreover, the latch also serves to convert the voltage output from the inverter chain to a current, and thereafter provide amplification to meet the specification. The clock enabled transistor M7, controls when the current is supplied to the display bars. Figure 7b shows the simulated variation of the current and voltage from the

latch. When the latch is off, negligible current is supplied to the display bar, however once the latch is on, a relatively constant current of ≥ 25 μA flows to the bars, as required for optimum luminesce. Moreover, the voltage across the display bar is initially constant at a specified value of 1.1 V, so as to allow the bars to turn on, and remains above this range with time.

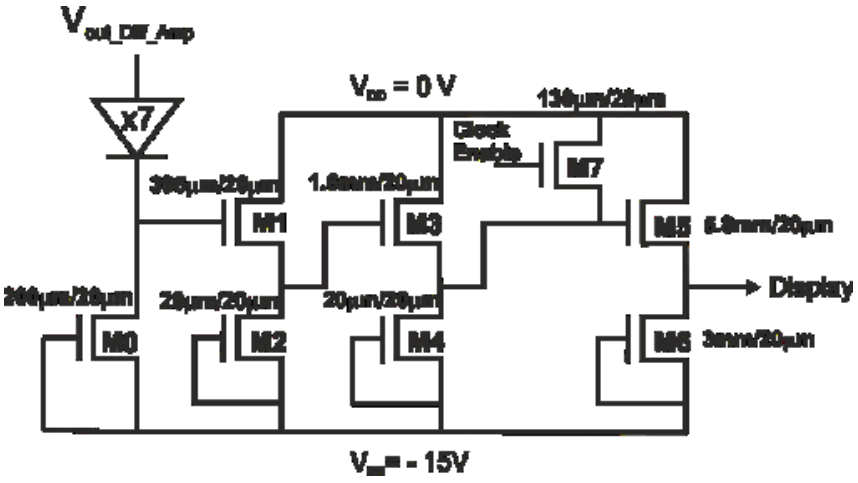

(a)

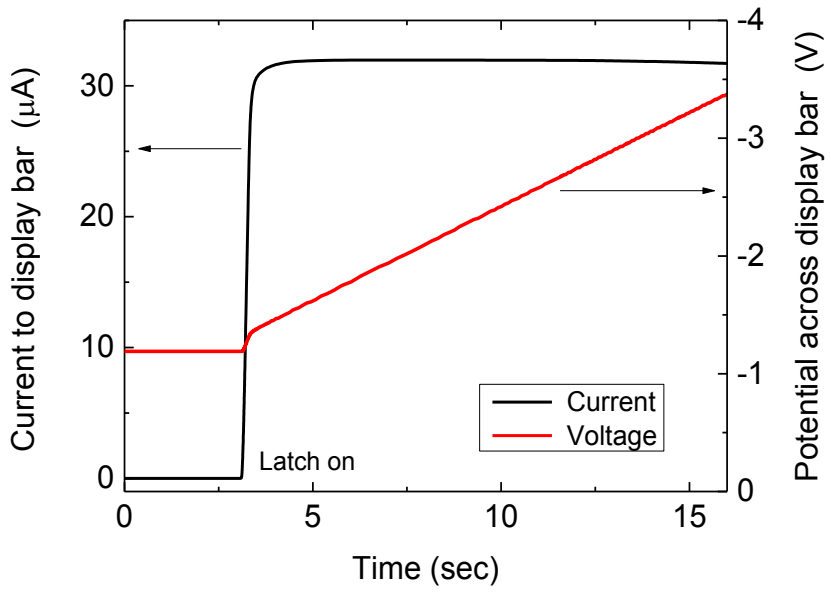

(b)

Fig. 7 *Organic Latch*

(a) Schematic diagram of the latch connected to the display.

(b) Simulation of the variation of current and voltage from a latch with respect to time.

3.4 Functionality of the Organic Op-Amp

The overall functionality of the organic circuit, comprising of the Op-Amp with a 7-stage inverter chain and a latch, for use in quantification of cholesterol levels is simulated, as in Fig. 8. The output voltage ranges between -1.8 V to -8.5 V, with linear scaling of about -0.7 V, between each milliMolar of cholesterol. Such linear scaling reflects the initial measurements in Fig. 2, from the electrochemical cell. The output voltage range can be enhanced further by reducing the contact resistance of the OTFTs, which strongly depends on the potential barriers between the organic semiconductor and the source/drain contacts.

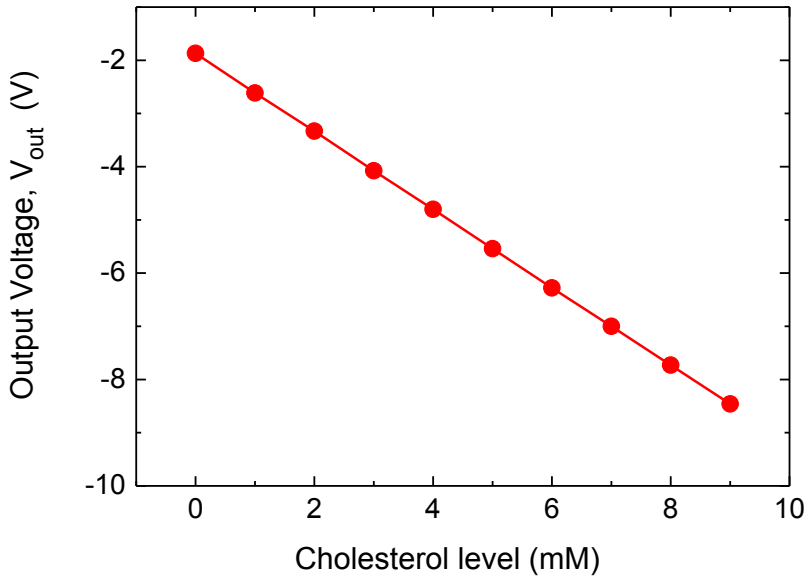

Fig. 8 *Simulation of the ouput voltage from the organic circuit with changes in cholesterol levels, with a linear quantification factor of 0.7 V/mM.*

4 Conclusion

An organic analog circuit with saturated load PMOS architecture was designed to signify changes in sampled cholesterol levels, from an electrochemical cell, in the range of 0 – 9 mM. The circuit comprised of a current source and differential amplifier, in conjugation with a 7-stage inverter chain and a latch. The designs were simulated with the aid of revised conventional model and parameters, so as to reflect the properties of the OTFT. The

amplifier operated with a highest open loop gain of 83 dB, and a close loop gain in the range of 26 – 39 dB, with corresponding bandwidth of 302 – 275 Hz respectively. At a maximum gain of 39 dB, the bandwidth was 275 Hz, resulting in gain-bandwidth product of 10.63 kHz. This value is currently the highest reported in the literature for a lower supply voltage of ±15 V. Moreover, the output voltage from the circuit showed linear scaling with changes in cholesterol level, with a quantification factor of -0.7 V/mM. Such practical results validate the implementation of the proposed organic circuit design, as key functional block in a cholesterol sensor system. The development of such systems, for point-of-care diagnostics, is becoming ever more attractive, as it allows regular monitoring of personal health, at a low-costs and user's convenience, with significant potential in enhancing overall health of patients.

5 Acknowledgments

The authors would like to thank the European Commission for provision of funds under the FP7 programme, in support of the interdisciplinary SIMS research project number 257372. The authors would also like to extend their appreciation to SIMS consortium for their valuable technical discussions.

6 References

1 Li, H. G., Yin, X. Y., Zhang, Z. Y.: ‚High-Precision Mixed Modulation DAC for an 8-Bit AMOLED Driver IC', J. Disp. Techn., 2015, **11**, (5), pp. 423-429

2 Taylor, D. M., Patchett, E. R., Williams, A., *et al*.: 'Fabrication and simulation of organic transistors and functional circuits', Chem. Phys., 2015, 456, pp. 85-92

3 Raiter, D., van Lieshout, P., van Roermund, A., Cantatore, E.: 'Positive-Feedback Level Shifter Logic for Large-Area Electronics, IEEE J. Sol. Stat. Circ., 2014, **49**, (2), pp. 524-535

4 Guerin, M., Berferet, E., Bènevent, E., *et al*.: 'Organic Complementary Logic Circuits and Volatile Memories Integrated on Plastic Foils', IEEE Trans. on Electr. Dev., 2013, **60**, (6), pp. 2045-2051

5 Gentili, D., Sonar, P., Liscio, F., *et al*.: 'Logic gate Devices on Printed Polymer Semiconducting Nanostripes', Nano Lett., 2013, **13**, (8), pp. 3643-3647

6 Chang, J., Zhang, X., Ge, T., Zhou, J.: 'Fully printed electronics on flexible substrates: High gain amplifier and DAC', Organ. Electr., 2014, **15**, (3), pp. 701-710

7 Marien, H., Steyaert, M., Heremans, P.: 'Analog Organic Electronics-Building Blocks for Organic Smart Sensor Systems', (Springer, New York, 2013), pp. 59-92

8 Zaki, T., Ante, F., Zschieschang, U., *et al*.: 'A 3.3 V 6-Bit 100 kS/s Current-Steering Digital-to-Analog Converter Using Organic P-Type Thin-Film Transistors on Glass', IEEE J. Sol. Stat. Circ., 2012, **47**, (1), pp. 292-300

9 Marien, H., Steyaert, M., van Veenendaal, E., Heremans, P.: 'A Fully Integrated $\Delta\Sigma$ ADC in Organic Thin-Film Transistor Technology on Flexible Plastic Foil', IEEE J. Sol. Stat. Circ., 2011, **46**, (1), pp. 276-284

10 Xiong, W., Guo, Y., Murmann, B.: 'A 3V, 6-bit C-2C Digital-to-Analog Converter using Complementary Organic Thin-Film Transistors on Glass', IEEE J. Sol. Stat. Circ., 2010, **45**, (7), pp. 1380-1388

11 Xiong, W., Zschieschan, U., Klauk, H., Murmann B.: 'A 3V 6-bit successive-approximation ADC using complementary organic thin-film transistors on glass', ISSCC Dig. Tech. Papers, San Francisco, CA, USA, Feb 2010, pp. 134-135

12 DiBenedetto, S., Facchetti, A., Ratner, M., Marks, T.: 'Molecular Self-Assembled Monolayers and Multilayers for Organic and Unconventional Inorganic Thin-Film Applications', Adv. Mat., 2009, **21**, pp. 1407-1433

13 Hwang, D., Oh, M., Hwang, J., Kim, J., Im, S.: 'Hysteresis mechanisms of pentacene thin-film transistors with polymer/oxide bilayer gate dielectrics', App. Phys. Lett., 2008, **92**, (1), pp. 013304

14 Gu, G., Kane, M.: 'Moisture induced electron traps and hysteresis in pentacene based organic thin-film transistors', Appl. Phys. Lett., 2008, **92**, (5), pp. 053305

15 Lee, S., Koo, B., Shin, J., *et al*.: 'Effects of hydroxyl groups in polymeric dielectrics on organic transistor performance', Appl. Phys. Lett., 2006, **88**, (16), pp. 162109

16 Campbell, G., Mutharasan, R.: 'Monitoring of the Self-Assembled Monolayer of 1-Hexadecanethiol on a Gold Surface at Nanomolar Concentration Using a Piezo-Excited Millimeter-Sized Cantilever Sensor', Langmuir, 2005, **21**, (25), pp. 11568-11573

17 Gu, G., Kane, M., Doty, J., Firester, A.: 'Electron traps and hysteresis in pentacene-based organic thin-film Transistors', Appl. Phys. Lett., 2005, **87**, (24), pp. 243512

18 Dimitrakopoulos, C., Mascaro, D.: 'Organic thin- film transistors: A review of recent advances', IBM J. Res. Dev., 2001, **45**, pp. 11-27

19 Bao, Z., Dodabalapur, A., Lovinger, A. J.: 'Soluble and Processable Regioregular Poly(3-hexylthiophene) for Thin Film Field-Effect Transistor Applications with High Mobility', Appl. Phys. Lett., 1996, **69**, (26), pp. 4108-4110

20 Noguchi, Y., Sekitani, T., Someya, T.: 'Organic-transistor-based flexible pressure sensors using ink-jet-printed electrodes and gate dielectric layers', Appl. Phys. Lett., 2006, **89**, (25), pp. 253507

21 Wang, L., Fine, D., Dodabalapur, A.: 'Nanoscale chemical sensor based on organic thin-film transistors', Appl. Phys. Lett, 2004, **85**, (26), pp. 6386-6388

22 Lee, Y., Sheu, C., Hsiao, R.: 'Gas sensing characteristics of copper phthalocyanine films: effects of film thickness and sensing temperature', Sens. Actu. B: Chem., 2004, **99**, (2-3), pp. 281-287

23 Evans, S., Johnson, S., Cheng Y., Shen, T.: 'Vapour sensing using hybrid organic–inorganic nanostructured materials', J. Mat. Chem., 2000, **10**, pp. 183-188

24 Someya, T., Sekitani, T., Iba, S., *et al*.: 'A large-area, flexible pressure sensor matrix with organic field-effect transistors for artificial skin application', Proc. Nat. Acad. Scie. U.S.A., 2004, **101**, (27), pp. 9966-9970

25 Maiellaro, G., Ragonese, E., Castorina, A., *et al*.: 'High-Gain Operational Transconductance Amplifiers in a Printed Complementary Organic TFT Technology on Flexible Foil', IEEE Trans. Circ. Syst., 2013, **60**, (12), pp. 3117-3125

26 Marien, H., Steyaert, M. S. J., van Veenendaal, E., Heremans, P.: 'Analog building blocks for organic smart sensor systems in organic thin-film transistor technology on flexible plastic foil', IEEE J. Sol. Stat. Circ., 2012, **47**, (7), pp. 1712-1720

27 Guerin, M., Daami, A., Jacob, S., *et al*.: 'High-gain fully printed organic complementary circuits on flexible plastic foils', IEEE Trans. Electr. Dev., 2011, **58**, (10), pp. 3587-3593

28 Nausieda, I., Ryu, K. K., Da He, D., *et al*.: 'Mixed-signal organic integrated circuits in a fully photolithographic dual threshold voltage technology', IEEE Trans. Electr. Dev., 2011, **58**, (3), pp. 865-873

29 Vaidya, V., Wilson, D. M., Zhang, X., Kippelen, B.: 'An Organic Complementary Differential Amplifier for Flexible AMOLED Applications', Proc. IEEE Intern. Symp. Circ. Syst., May 2010, pp. 3260-3260

30 Raja, M., Donaghy, D., Myers R., Eccleston, W.: 'Impact of universal mobility law on polycrystalline organic thin-film transistors', J. Appl. Phys., 2012, **112**, pp. 084503

31 Raja, M., Eccleston, W.: 'Analytical device models for disordered organic Schottky diode and thin-film transistors for circuit simulations', IET Circ. Dev. Syst., 2012, **6**, (2), pp. 122-129

32 Meixner, R., Göbel, H., Qiu, H., *et al*.: 'A Physical-Based PSPICE Compact Model for Poly(3-hexylthiophene) Organic Field-Effect Transistors', *IEEE Trans. Electr. Dev.,* 2008, **55**, (7), pp. 1776-1781

33 Metrohm, 'Autolab Application Note EC08' (Metrohm 2011), pp. 1-3.

34 Ahmadraji, T., Gonzalez-Macia, L., Killard, A. J.: 'A biosensor for the determination of high density lipoprotein cholesterol employing combined surfactant-derived selectivity and sensitivity enhancements', Analyt. Meth., 2014, 6, (12), pp. 3975-3981

35 Eccleston, W.: "Analysis of current flow in polycrystalline TFTs", IEEE Trans. on Elect. Dev., 2006, **53**, (3), pp. 474-480

36 Razazi, B.: 'Design of analog CMOS Integrated Circuits', (McGraw-Hill Education, 2017, 2nd edn.), pp. 100-118

37 Allen, P. E.: http://www.aicdesign.org/SCNOTES/2005notes/Chapter05-Web(8_3_05).pdf, pp. 5.1-6, March 2005, accessed October 2010